electronics

IMPACT FACTOR 2.9

CITESCORE 4.7

Article

# Robust Adaptive Beamforming for Interference Suppression Based on SNR

Lin Chang, Hao Zhang, T. Aaron Gulliver and Tingting Lyu

MDPI

https://doi.org/10.3390/electronics12214501

*electronics*

MDPI

*Article*

# Robust Adaptive Beamforming for Interference Suppression Based on SNR

**Lin Chang [1], Hao Zhang [1,*], T. Aaron Gulliver [2] and Tingting Lyu [1]**

[1] Faculty of Information Science and Engineering, Ocean University of China, Qingdao 266400, China; changlin@stu.ouc.edu.cn (L.C.); tingtinglu@ouc.edu.cn (T.L.)
[2] Department of Electrical and Computer Engineering, University of Victoria, Victoria, BC V8W 2Y2, Canada; agullive@ece.uvic.ca
* Correspondence: zhanghao@ouc.edu.cn

**Abstract:** Robust adaptive beamforming (RAB) can be used to suppress interference signals while retaining the desired signals received by a sensor array. However, desired signal self-cancellation and model mismatch can affect RAB performance. In this paper, a novel interference-plus-noise covariance matrix (INCM) reconstruction method is proposed for RAB to solve these problems. The proposed method divides the desired signal into two ranges according to the input signal-to-noise ratio (SNR), namely low SNR and high SNR. In the low SNR range, INCM reconstruction directly uses the same sample covariance matrix as the sample matrix inversion (SMI) beamformer to retain the advantages of the traditional SMI algorithm. In the high SNR range, the eigenvalues of the sample covariance matrix are used to estimate the interference power and noise power. The optimized interference steering vector (SV) is obtained by solving a quadratic convex optimization problem in an interference subspace. The INCM is reconstructed from the interference SVs, interference power, and noise power. The reconstructed INCM is then used to correct the desired signal SV via maximizing the beamformer output power. This is achieved by solving a quadratically constrained quadratic programming (QCQP) problem. Analysis and simulation results are presented which demonstrate that the proposed method performs well under a variety of mismatch conditions.

**Keywords:** robust adaptive beamforming; SNR estimation; interference covariance matrix reconstruction; subspace selection



**Citation:** Chang, L.; Zhang, H.; Gulliver, T.A.; Lyu, T. Robust Adaptive Beamforming for Interference Suppression Based on SNR. *Electronics* **2023**, *12*, 4501. https://doi.org/10.3390/electronics12214501

Academic Editor: Walter Ciccognani

Received: 22 September 2023
Revised: 18 October 2023
Accepted: 25 October 2023
Published: 1 November 2023



## 1. Introduction

In some application scenarios, such as target detection [1,2], target recognition [3,4], and communications [5,6], ambient noise and interference will degrade the quality of desired signals [7]. Beamforming [8–10] can be employed to reduce the effects of noise and interference and improve the signal-to-noise ratio (SNR).

In recent decades, adaptive beamforming has been used in many fields to improve signal quality [11,12]. The optimal beamformer for maximizing the output signal-to-interference-plus-noise ratio (SINR) is known as the minimum variance distortionless response (MVDR) beamformer [13]. The key to the efficiency of MVDR beamforming is the signal of interest (SOI) in the training data. Both the convergence rate and performance of the adaptive beamforming algorithm are decreased when the training data contains the SOI [14,15]. However, the sample covariance matrix is often corrupted by the SOI in many practical applications, such as radio astronomy, mobile communications, and passive source location [14]. Further, MVDR beamforming is sensitive to steering vector (SV) mismatch, mainly when the input SNR is high [16]. In practical problems, this mismatch can be caused by factors such as sensor position errors, signal direction errors, amplitude and phase errors, and local scattering.

In order to improve the robustness of beamforming, various robust adaptive beamforming algorithms (RABs) have been proposed. Diagonal loading (DL) [17–19] employs

sampling covariance processing and adds a quadratic restriction on the SV or a scaled identity matrix to the sample covariance matrix (SCM). However, an appropriate DL factor must be selected. The eigenspace-based algorithm [20–23] is a practical algorithm to improve the robustness of beamforming. It can optimize the SV [20] or enhance the accuracy of the covariance matrix [21] through subspace projection. The challenge with this technique is determining the desired subspace. The method based on the uncertainty set constraint [14,24] is applicable to a variety of mismatch conditions, but it has high computational complexity and cannot always have an ideal output in a wide SNR range.

In recent years, the interference-plus-noise covariance matrix (INCM) reconstruction method has been proposed to reduce the SOI influence and improve the robustness of adaptive beamformers. INCM reconstruction was initially proposed in [25] and employs the Capon power spectrum integrated over a complement region of the SOI direction. Then, the INCM is used in a QCQP problem to estimate the SV of the desired signal. A low complexity algorithm that reconstructs the INCM based on spatial power spectral sampling was proposed in [26]. The effect of interference power estimation on INCM reconstruction was analyzed in [27], and a simplified algorithm was developed to estimate the interference power. In [28], an RAB approach was proposed to reconstruct the INC matrix based on power method processing and spatial spectrum matching, which can avoid over-complicated calculations. Although these INCM algorithms improve the robustness of beamforming, the existence of look direction or other SV errors degrades their performance.

In this paper, a new INCM reconstruction method is proposed to improve beamforming performance in various environments. First, the output characteristics of the sample matrix inversion (SMI) beamformer [29] at different input SNRs are analyzed. This is important because INCM reconstruction methods have been designed for different SNR ranges according to these characteristics. The reconstructed INCM is replaced by the SCM when the input SNR is low. When the input SNR is high, the estimated interference power, corresponding SV, and estimated noise power are used to reconstruct the INCM. In addition, the presumed SV of the signal is corrected by solving a QCQP problem. The weight vector of the proposed beamformer is obtained by combining the reconstructed INCM and the presumed SV. The main contributions include:

1. This paper proposes an estimation method of SNR, and different INCM reconstruction methods are employed for different SNRs, which reduces the complexity generated by solving several QCQP problems and improves the output performance of beamforming at low SNR.
2. An automatic subspace determination method is proposed to reconstruct INCM in the high SNR range. Compared with the algorithm that relies on empirical subspace selection, this method avoids the detrimental effect of the number of signals and elements on the subspace selections. It improves the robustness of the subspace-based reconstruction INCM algorithm.

The remainder of this paper is organized as follows. Section 2 presents the system model and MVDR beamforming problem. The impact of the input SNR on the SMI beamformer is analyzed in Section 3, in which INCM reconstruction based on the input SNR and SOI SV estimation are also described. Simulation results are presented in Section 4 to illustrate the effectiveness of the proposed approach. Finally, some conclusions are given in Section 5.

*Notation:* Uppercase bold letters are used to denote matrices, and lowercase bold letters denote column vectors. $(\cdot)^T$, $(\cdot)^H$, $E\{\cdot\}$, and $\|\cdot\|_2$ denote transpose, conjugate transpose, expectation, and Euclidean norm, respectively.

## 2. Background

Consider a receiver with a uniform linear array (ULA) and $M$ sensors. $P$ far field plane wave narrowband signals impinge on this array from the directions $\theta_1, \ldots, \theta_P$. The received signals at time $k$ in the array $\mathbf{x}(k) = [x_1(k), x_2(k), \ldots, x_M(k)]^T$ can be expressed as:

$$\mathbf{x}(k) = \mathbf{x}_s(k) + \mathbf{x}_i(k) + \mathbf{x}_n(k) \tag{1}$$

where $\mathbf{x}_s(k) = \mathbf{a}_1 s_1(k)$ is the SOI, $\mathbf{x}_i(k) = \sum_{i=2}^{P} \mathbf{a}_i s_i(k)$ is the interference, and $\mathbf{x}_n(k)$ is noise. It is assumed that the SOI, interference, and noise are statistically independent. The actual SV for the signals $s_i(k)$ from $\theta_i$, $i = 1, 2, \ldots, P$, can be expressed as:

$$\mathbf{a}_i = \left[1, e^{-j2\pi d \sin\theta_i/\varepsilon}, \ldots, e^{-j2\pi(M-1)d \sin\theta_i/\varepsilon}\right]^T, \tag{2}$$

where $j = \sqrt{-1}$, $\varepsilon$ is the wavelength of the signal wavefront, and $d$ is the distance between adjacent elements. The vector $\mathbf{x}_n(k)$ is assumed to be complex white Gaussian noise with zero mean and variance $\sigma_n^2$. The output of the beamformer is:

$$\mathbf{y}(k) = \mathbf{w}^H \mathbf{x}(k), \tag{3}$$

where $\mathbf{w} = [w_1, w_2, \ldots, w_M]^T$ is the weight vector.

The optimal weight vector $\mathbf{w}$ can be obtained as the solution to the following signal-to-interference-plus-noise ratio (SINR) maximization problem:

$$SINR_{max} = \max \frac{\sigma_1^2 \left|\mathbf{w}^H \mathbf{a}_1\right|^2}{\mathbf{w}^H \mathbf{R}_{in} \mathbf{w}}, \tag{4}$$

where $\sigma_1^2 = E\{|s_1(k)|^2\}$ is the power of the SOI, and $\mathbf{R}_{in}$ is the INCM given by:

$$\begin{aligned} \mathbf{R}_{in} &= E\{[\mathbf{x}_i(k) + \mathbf{x}_n][\mathbf{x}_i(k) + \mathbf{x}_n]^H\} \\ &= \sum_{i=2}^{P} \sigma_i^2 \mathbf{a}_i {\mathbf{a}_i}^H + \sigma_n^2 \mathbf{I}, \end{aligned} \tag{5}$$

where $\sigma_i^2$ is the interference power, and $\mathbf{I}$ is the $M \times M$ identity matrix.

To maximize the output SINR, the output interference and noise should be minimized while not distorting the SOI. Then, the SINR maximization problem can be expressed as the following optimization problem:

$$\min_{\mathbf{w}} \mathbf{w}^H \mathbf{R}_{in} \mathbf{w} \quad \text{s.t. } \mathbf{w}^H \mathbf{a}_1 = 1 \tag{6}$$

with solution

$$\mathbf{w}_{opt} = \frac{\mathbf{R}_{in}^{-1} \mathbf{a}_1}{{\mathbf{a}_1}^H \mathbf{R}_{in}^{-1} \mathbf{a}_1}. \tag{7}$$

This is known as the minimum variance distortionless response (MVDR) beamformer or the standard Capon beamformer. In practice, the exact $\mathbf{R}_{in}$ is not available and so is usually replaced with the sample covariance matrix (SCM) $\hat{\mathbf{R}}$, which is estimated as the average of $K$ snapshots:

$$\hat{\mathbf{R}} = \frac{1}{K} \sum_{k=1}^{K} \mathbf{x}(k) \mathbf{x}^H(k). \tag{8}$$

In this case, the MVDR beamformer is the SMI beamformer. Due to array errors, the exact $\mathbf{a}_1$ cannot be obtained. Since the array geometry is known, denote the initial

approximate SVs of the desired signal and interference obtained using the DOA estimation as $\bar{\mathbf{a}}_s$ and $\bar{\mathbf{a}}_l$, $l = 2, \ldots, P$, respectively. The corresponding optimal solution is:

$$\mathbf{w}_{SMI} = \frac{\hat{\mathbf{R}}^{-1}\bar{\mathbf{a}}_s}{\bar{\mathbf{a}}_s^H \hat{\mathbf{R}}^{-1}\bar{\mathbf{a}}_s}. \tag{9}$$

The SOI is typically included in the SCM using:

$$\hat{\mathbf{R}} = \hat{\mathbf{R}}_\mathbf{s} + \hat{\mathbf{R}}_{in} + \hat{\mathbf{R}}_{cross}, \tag{10}$$

where $\hat{\mathbf{R}}_\mathbf{s}$, $\hat{\mathbf{R}}_{in}$, and $\hat{\mathbf{R}}_{cross}$ are the estimated SOI covariance matrix, INCM, and cross-covariance matrix between the desired signal and interference-plus-noise components, respectively, which can be expressed as:

$$\hat{\mathbf{R}}_s = \frac{1}{K}\sum_{k=1}^{K} \mathbf{x}_s(k)\mathbf{x}_s{}^H(k) \tag{11}$$

$$\hat{\mathbf{R}}_{in} = \frac{1}{K}\sum_{k=1}^{K} (\mathbf{x}_i(k) + \mathbf{x}_n(k))(\mathbf{x}_i(k) + \mathbf{x}_n(k))^H \tag{12}$$

$$\hat{\mathbf{R}}_{cross} = \frac{1}{K}\sum_{k=1}^{K} \mathbf{x}_s(k)(\mathbf{x}_i(k) + \mathbf{x}_n(k))^H + (\mathbf{x}_i(k) + \mathbf{x}_n(k))\mathbf{x}_s^H(k). \tag{13}$$

The SOI exists in both $\hat{\mathbf{R}}_s$ and $\hat{\mathbf{R}}_{cross}$. However, as the quantity of snapshots rises, $\hat{\mathbf{R}}_{cross}$ approaches zero, and $\hat{\mathbf{R}}$ approaches the actual covariance matrix.

## 3. Proposed Method

It can be seen from (9) and (10) that, when the SOI is present in $\hat{\mathbf{R}}$, signal self-cancellation will occur, and this cancellation increases as the input SNR increases. In addition, inaccurate estimation of $\bar{\mathbf{a}}_s$ also affects the solution to $\mathbf{w}$. Thus, the goal in this section is to select a suitable method for INCM reconstruction according to the input SNR and optimize the SOI SV based on this reconstruction.

### *3.1. Input SNR Impact on the SMI Beamformer*

According to (7) and (9), the SMI beamformer can be regarded as an approximation of the MVDR algorithm. Figure 1 presents the output SINR versus input SNR of this beamformer, and Figure 2 shows the SMI performance when there are amplitude and phase perturbations, as well as look direction and sensor location errors. The look direction error is assumed to be uniformly distributed in $[-4^\circ, 4^\circ]$. The gain error and phase error are randomly distributed according to $N(0, 0.1^2)$ and $N(0, 0.25\pi^2)$, respectively, and the sensor location error is uniformly distributed in the interval $[-0.1, 0.1]$ measured in sensor space. This shows that, when the input SNR is less than 0 dB, the algorithm performs well, but when the SNR is greater than 0 dB, there is a decrease in the output SINR. Thus, 0 dB is considered to divide the SNR range.

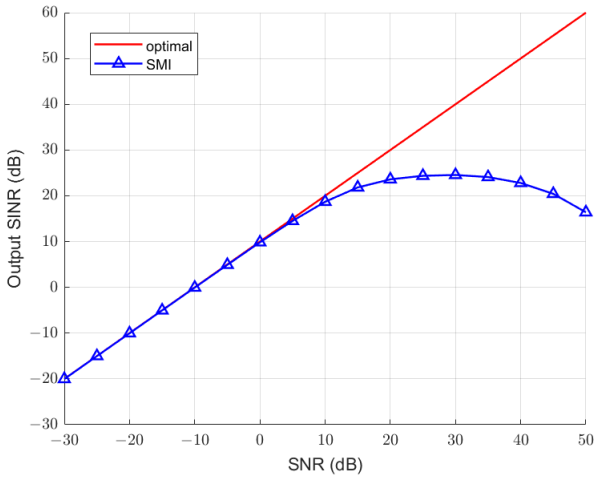


**Figure 1.** Output SINR versus input SNR of the SMI beamformer.

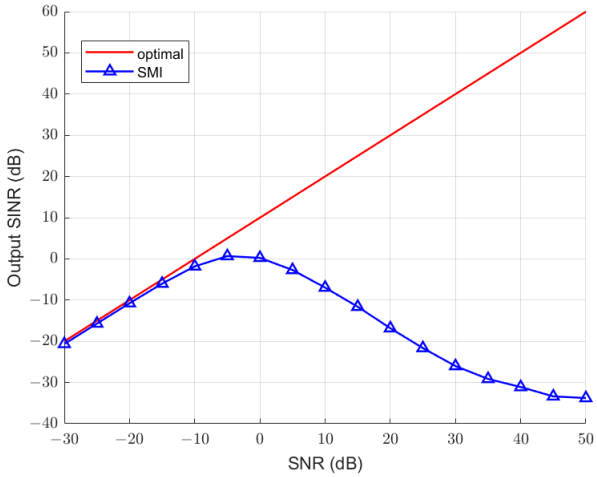


**Figure 2.** Output SINR versus input SNR of the SMI beamformer with perturbations and errors.

### *3.2. INCM Reconstruction*

The INCM reconstruction aims to eliminate SOI components while retaining interference-plus-noise elements. When the SOI SNR is small, the SOI component in the SCM is small, so the SCM can be used directly instead of the INCM. When the SOI SNR is large, the INCM can be reconstructed using the estimated interference power, noise power, and interference signal SVs.

The covariance matrix of $\mathbf{x}(k)$ is:

$$\mathbf{R} = \sum_{i=1}^{P} \sigma_i^2 \mathbf{a}_i {\mathbf{a}_i}^H + \sigma_n^2 \mathbf{I}. \tag{14}$$

This can also be expressed using eigenvalue decomposition (EVD) as:

$$\mathbf{R} = \sum_{i=1}^{M} \lambda_i \mathbf{e}_i \mathbf{e}_i^H, \tag{15}$$

where $\lambda_1 \geq \lambda_2 \geq \ldots \geq \lambda_P > \lambda_{P+1} = \ldots = \lambda_M = \sigma_n^2$ are the eigenvalues of $\mathbf{R}$, and $\mathbf{e}_i$ is the eigenvector corresponding to $\lambda_i$. Further, (15) can be rewritten as:

$$\begin{aligned}\mathbf{R} &= \sum_{i=1}^{P} \lambda_i \mathbf{e}_i \mathbf{e}_i^H + \sigma_n^2 \sum_{i=P+1}^{M} \mathbf{e}_i \mathbf{e}_i^H \\ &= \sum_{i=1}^{P} \lambda_i \mathbf{e}_i \mathbf{e}_i^H + \sigma_n^2 \mathbf{I} - \sigma_n^2 \sum_{i=1}^{P} \mathbf{e}_i \mathbf{e}_i^H \\ &= \sum_{i=1}^{P} (\lambda_i - \sigma_n^2) \mathbf{e}_i \mathbf{e}_i^H + \sigma_n^2 \mathbf{I}.\end{aligned} \tag{16}$$

Comparing (14) and (16), we obtain:

$$\sum_{i=1}^{P} \sigma_i^2 \mathbf{a}_i {\mathbf{a}_i}^H = \sum_{i=1}^{P} (\lambda_i - \sigma_n^2) \mathbf{e}_i \mathbf{e}_i^H. \tag{17}$$

However, this relationship may not hold for a given value of $i$. Since each signal SV $\mathbf{a}_i$ corresponds to a unique signal, and each large eigenvalue also corresponds to a unique signal, the correspondence between the two sides of the equation can be determined by calculating the correlation between $\mathbf{a}_i$ and $\mathbf{e}_i$. For the steering vector $\mathbf{a}_p$ of the $p$th signal, its correlation with the $i$th eigenvector $\mathbf{e}_i$ can be calculated as:

$$c_i = \frac{|\mathbf{e}_i^H \mathbf{a}_p|}{\|\mathbf{e}_i\| \|\mathbf{a}_p\|} \qquad i = 1, 2, \ldots, P. \tag{18}$$

Since ${\mathbf{a}_p}^H \mathbf{a}_p = M$, ${\mathbf{e}_i}^H \mathbf{e}_i = 1$, (18) becomes:

$$c_i = |\mathbf{e}_i^H \mathbf{a}_p|. \tag{19}$$

Denote the eigenvector that maximizes $c_i$ in (19) as $\mathbf{e}_{pc}$ and the corresponding eigenvalue as $\lambda_{pc}$. Then, from (17), we have:

$$\sigma_p^2 \mathbf{a}_p {\mathbf{a}_p}^H = (\lambda_{pc} - \sigma_n^2) \mathbf{e}_{pc} \mathbf{e}_{pc}^H. \tag{20}$$

The relationship between the signal power and eigenvalues can be expressed as:

$$\sigma_p^2 = \frac{(\lambda_{pc} - \sigma_n^2)}{M}. \tag{21}$$

Therefore, the approximate signal power $p_s$ and interference power $p_l$, $l = 2, \ldots, P$, in the received signal can be expressed as:

$$\begin{aligned} p_s &= \frac{(\hat{\lambda}_{sc} - \sigma_n^2)}{M} \\ p_l &= \frac{(\hat{\lambda}_{lc} - \sigma_n^2)}{M}. \end{aligned} \tag{22}$$

If the signal power is much greater than the noise power, $\sigma_n^2$ in (22) can be ignored, and (22) can be rewritten as:

$$\begin{aligned} p_s &= \frac{\hat{\lambda}_{sc}}{M} \\ p_l &= \frac{\hat{\lambda}_{lc}}{M}, \end{aligned} \tag{23}$$

where $\hat{\lambda}_i$ is the eigenvalue of $\hat{\mathbf{R}}$, and $\hat{\lambda}_{sc}$ and $\hat{\lambda}_{lc}$ are the eigenvalues corresponding to the desired signal power $\sigma_1^2$ and interference power $\sigma_l^2$ in (20). The estimated noise power $p_n$ is:

$$p_n = \frac{1}{M-P} \sum_{i=P+1}^{M} \hat{\lambda}_i. \tag{24}$$

The actual SNR is equal to $10 \log_{10} \sigma_1^2 / \sigma_n^2$. Using (22) and (24) gives the following approximation:

$$SNR_b = 10 \log_{10} p_s / p_n. \tag{25}$$

According to the division of the SNR range by 0 dB in Section 3.1, when $SNR_b \leqslant 0$, the input SNR is small, and $\hat{\mathbf{R}}$ can be used in place of the reconstructed INCM $\hat{\tilde{\mathbf{R}}}_{in}$. When $SNR_b > 0$, the input SNR is high, and the INCM can be reconstructed using (5).

In the high input SNR region, the SVs are first optimized using the method in [30] to obtain the coarsely optimized SOI SV $\hat{\mathbf{a}}_s$ and interference SVs $\hat{\mathbf{a}}_l$. Then, a more accurate interference SV $\hat{\tilde{\mathbf{a}}}_l$ can be obtained using the orthogonality of the interference subspace. The interference subspace can be realized by constructing a matrix $\mathbf{\Phi}$ in the interference interval:

$$\mathbf{\Phi} = \int_{\Theta_i} \bar{\mathbf{a}}_l(\theta) \bar{\mathbf{a}}_l^H(\theta) d\theta, \tag{26}$$

where $\Theta_i$ is the angular sector that contains the interference, and $\bar{\mathbf{a}}_l(\theta)$ is the SV associated with $\theta$ in $\Theta_i$ based on the known array structure.

The EVD of $\mathbf{\Phi}$ is:

$$\mathbf{\Phi} = \sum_{i=1}^{M} \tau_i \mathbf{h}_i {\mathbf{h}_i}^H, \tag{27}$$

where $\tau_1 \geq \tau_2 \geq \ldots \geq \tau_M$ are the eigenvalues of $\mathbf{\Phi}$, and $\mathbf{h}_i$ is the eigenvector corresponding to $\tau_i$. Let $\mathbf{H}_1 = [\mathbf{h}_1, \mathbf{h}_2, \ldots, \mathbf{h}_q]$ be the eigenvector matrix composed of the largest $q$ eigenvalues.

If $q$ is chosen appropriately, $\mathbf{H}_1$ can represent the interference subspace. Then, the projection on the subspace spanned by $\mathbf{H}_1$ can largely eliminate the desired signal while retaining the interference components [31] so that:

$$\mathbf{H}_1 \mathbf{H}_1^H \hat{\mathbf{a}}_s \approx \mathbf{0} \tag{28}$$

and

$$\mathbf{H}_1 \mathbf{H}_1^H \hat{\mathbf{a}}_l \approx \hat{\mathbf{a}}_l. \tag{29}$$

In the existing algorithms, the appropriate number of subspaces $q$ is usually selected based on experience. However, for different numbers of array elements and signal source information, the determination of this subspace needs to be more flexible. This paper proposes a method for determining the subspace autonomously, which can use the relationship in (29) to find an appropriate value of $q$. Define

$$\delta(m) = \|\mathbf{H}_1(m) \mathbf{H}_1^H(m) \hat{\mathbf{a}}_l\|_2^2 - \|\hat{\mathbf{a}}_l\|_2^2, \quad m = 2, 3, \ldots, M-1, \tag{30}$$

where $\mathbf{H}_1(m) = [\mathbf{h}_1, \mathbf{h}_2, \ldots, \mathbf{h}_m]$, and when $\mathbf{H}_1(m)$ satisfies (29), $\delta(m), \delta(m+1), \ldots, \delta(M-1)$ are negligible. However, it is usually challenging to determine if the value of $\delta(m)$ is negligible. Given that $g(m) = |\delta(m-1)/\delta(m)|$, the value of $g(m)$ can judge the change in $\delta(m)$. Figure 3 shows the value of $g$ and $\delta$ versus $m$. If $\delta(m)$ is negligible and $\delta(m-1)$ is not close to zero, the difference between $\delta(m-1)$ and $\delta(m)$ will be significant, so $g(m)$ is the maximum for all $g(\cdot)$.

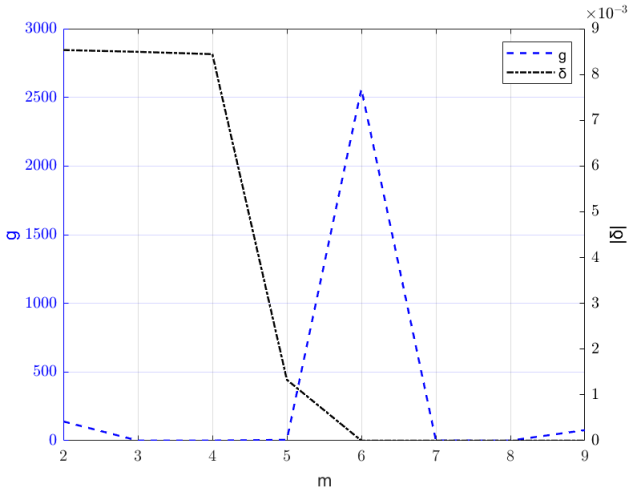


**Figure 3.** Values of $g$ and $\delta$ versus $m$.

Choosing $q = \arg\max |g(m)|$, the projection matrix $\mathbf{Z} = \mathbf{Z}^H = \mathbf{H}_1(q)\mathbf{H}_1^H(q)$ will satisfy (29) while keeping the left-hand side of (28) small. Furthermore, the complement subspace $\mathbf{\Psi} = \mathbf{I} - \mathbf{Z}$ is orthogonal to the actual interference SV $\mathbf{a}_l$, so:

$$\|\mathbf{\Psi}^H \mathbf{a}_l\| \approx 0 \quad l = 2, \ldots, P. \tag{31}$$

Using $\hat{\mathbf{a}}_l$, the orthogonality condition in (31) is replaced by $\|\mathbf{\Psi}^H \hat{\mathbf{a}}_l\| > 0$, which gives:

$$\|\mathbf{\Psi}^H(\hat{\mathbf{a}}_l + \mathbf{v}_l)\|_2^2 < \|\mathbf{\Psi}^H \hat{\mathbf{a}}_l\|_2^2, \tag{32}$$

where $\mathbf{v}_l$ is the mismatch of $\hat{\mathbf{a}}_l$, and $\hat{\tilde{\mathbf{a}}}_l = \hat{\mathbf{a}}_l + \mathbf{v}_l$ is closer to $\mathbf{a}_l$ than $\hat{\mathbf{a}}_l$.

Using an approach similar to that in [31], $\hat{\tilde{\mathbf{a}}}_l$ can be obtained by solving the following problem:

$$\begin{aligned} \min_{\mathbf{v}_{l\perp}} \quad & (\hat{\mathbf{a}}_l + \mathbf{v}_{l\perp})^H \hat{\mathbf{R}}^{-1} (\hat{\mathbf{a}}_l + \mathbf{v}_{l\perp}) \\ s.t. \quad & \hat{\mathbf{a}}_l \mathbf{v}_{l\perp} = 0 \\ & \|\mathbf{\Psi}^H(\hat{\mathbf{a}}_l + \mathbf{v}_{l\perp})\|_2^2 < \|\mathbf{\Psi}^H \hat{\mathbf{a}}_l\|_2^2, \end{aligned} \tag{33}$$

where $\mathbf{v}_{l\perp}$ is the component of $\mathbf{v}_l$ orthogonal to $\hat{\mathbf{a}}_l$. The mismatch vector can be decomposed as $\mathbf{v}_l = \mathbf{v}_{l\perp} + \mathbf{v}_{l\|}$, where $\mathbf{v}_{l\|}$ is the component parallel to $\hat{\mathbf{a}}_l$. $\mathbf{v}_{l\|}$ is a scaled copy of $\hat{\mathbf{a}}_l$ and so does not affect the SINR; thus, it can be ignored in (33). The final corrected SVs are then:

$$\hat{\tilde{\mathbf{a}}}_l = \hat{\mathbf{a}}_l + \mathbf{v}_{l\perp}. \tag{34}$$

Combined with the estimated signal power obtained previously, the INCM is reconstructed as:

$$\hat{\tilde{\mathbf{R}}}_{in} = \sum_{l=2}^{P} p_l \hat{\tilde{\mathbf{a}}}_l \hat{\tilde{\mathbf{a}}}_l^H + p_n \mathbf{I}. \tag{35}$$

### *3.3. SV Estimation*

Using an approach similar to (33), a corrected desired signal SV $\hat{\tilde{\mathbf{a}}}_s$ can be obtained by solving the following QCQP problem:

$$\begin{aligned} \min_{\mathbf{v}_{s\perp}} \quad & (\breve{\mathbf{a}}_s + \mathbf{v}_{s_\perp})^H \hat{\tilde{\mathbf{R}}}_{in}^{-1} (\breve{\mathbf{a}}_s + \mathbf{v}_{s_\perp}) \\ s.t. \quad & \breve{\mathbf{a}}_s \mathbf{v}_{s\perp} = 0 \\ & (\breve{\mathbf{a}}_s + \mathbf{v}_{s_\perp})^H \hat{\tilde{\mathbf{R}}}_{in} (\breve{\mathbf{a}}_s + \mathbf{v}_{s_\perp}) < \breve{\mathbf{a}}_s^H \hat{\tilde{\mathbf{R}}}_{in} \breve{\mathbf{a}}_s, \end{aligned} \tag{36}$$

where $\mathbf{v}_{s\perp}$ is the orthogonal component of $\mathbf{v}_s$, and $\mathbf{v}_s$ is the mismatch of $\check{\mathbf{a}}_s$, where $\check{\mathbf{a}}_s = \bar{\mathbf{a}}_s$ when $SNR_b \leqslant 0$ and $\check{\mathbf{a}}_s = \hat{\mathbf{a}}_s$ when $SNR_b > 0$. Then the final corrected SV is $\hat{\check{\mathbf{a}}}_s = \check{\mathbf{a}}_s + \mathbf{v}_{s_\perp}$. After obtaining $\hat{\hat{\mathbf{R}}}_{in}$ and $\hat{\check{\mathbf{a}}}_s$, they can be substituted for $\hat{\mathbf{R}}^{-1}$ and $\bar{\mathbf{a}}_s$ in (9) to obtain:

$$\mathbf{w} = \frac{\hat{\hat{\mathbf{R}}}_{in}^{-1}\hat{\check{\mathbf{a}}}_s}{\hat{\check{\mathbf{a}}}_s^H\hat{\hat{\mathbf{R}}}_{in}^{-1}\hat{\check{\mathbf{a}}}_s}. \tag{37}$$

The computational complexity in the low SNR region is $\mathcal{O}(M^{3.5})$, due to the solution to the QCQP problem for SOI SV. In the high SNR region, the main complexity is in solving the QCQP problem for SOI SV and each interference SV, which has computational complexity $\mathcal{O}(PM^{3.5})$.

## 4. Performance Evaluation

In this section, simulation is employed to evaluate the performance of the proposed algorithm. The proposed method is compared with the INCM reconstruction beamformer of volume integration (INCM-volume) [32], INCM reconstruction via simplified interference power estimation [27] with desired signal steering vector estimation [20] (INCM-Simplified), beamforming using maximum entropy (INCM-MEPS) [33], beamformer based on an adaptive diagonal loading for the SMI (NDL-SMI) [34], INCM reconstruction beamformer based on a local maximum of the Capon power (INCM-MCP) [35], and INCM reconstruction beamformer based on subspace decomposition and steering vector correction (INCM-SDC) [36]. Narrowband continuous wave (CW) signals are considered, so both the SOI and interference are CW signals. A ULA with $M = 10$ omnidirectional sensors and half-wavelength spacing is employed as the passive sensor array. The additive noise is modeled as complex white Gaussian noise. The frequencies of the SOI and two interference signals are $f = 60$ kHz, $f_1 = 59$ kHz, and $f_2 = 61$ kHz, respectively. The SOI arrives from angle $\theta_1 = 5^\circ$ and the interference from angles $\theta_2 = -50^\circ$ and $\theta_3 = -20^\circ$. The interference-to-noise ratio (INR) in each sensor is 30 dB in all simulations, and the SOI is always present in the snapshot data. The SNR is 10 dB in the fixed input SNR experiments and $K = 2000$ in the fixed snapshots experiments.

The interference angular sector in the proposed method is:

$$\Theta_i = \Theta_1 \bigcup \Theta_2 = [\theta_2 - 5^\circ, \theta_2 + 5^\circ] \bigcup [\theta_3 - 5^\circ, \theta_3 + 5^\circ].$$

The angle sector of the desired signal is set to $\Theta_s = [\theta_1 - 5^\circ, \theta_1 + 5^\circ]$ for the method in [36]. All signal angular sectors use a uniform sample angular interval of $0.1^\circ$. The energy threshold for the methods in [20,30] is set to $\rho = 0.9$. The number of sampling points in $\Theta_{int}$ is $I = 40$ for the method in [32] and, for the method in [33], is $L = 50$ and $S = 10$. For the approach in [35], $\Delta\theta_l = 10^\circ, \tilde{\eta} = 0.1$, and the number of sample points is $2\tilde{\eta}/0.01$. The optimization problem is solved using CVX [37]. All simulation results are the average of 200 Monte Carlo trials.

The following SV errors are considered: look direction error, sensor gain error, phase error, and location perturbation. The $n$th element of the SV can then be expressed as:

$$(1 + \Delta\xi)e^{-j2\pi(nd+\Delta d)\sin(\theta+\Delta\theta)/\varepsilon}e^{-j\Delta\varphi}, \quad n = 0, 1, \ldots, M-1, \tag{38}$$

where $\Delta\xi$ is the gain error, $\Delta\varphi$ is the phase error, $\Delta\theta$ is the look direction error, and $\Delta d$ is the sensor location perturbation. The errors change with each trial but remain constant across all snapshots. In addition, the following experiments also consider the presence of coherent local scattering and the influence of different interference numbers on these algorithms.

### *4.1. Case 1: Known SV*

First, an ideal case is considered where the SV is known, so all errors are 0. Table 1 gives the estimated SNR of the proposed method at different input SNRs. The proposed method

can distinguish between low and high SNRs and also estimate the input SNR well when the actual input SNR is greater than −20 dB. Figure 4 presents the mean output SINR of the beamformers versus the input SNR for $K = 2000$ snapshots. Figure 5 shows the deviation of each beamformer from the optimal beamformer. This shows that the INCM-volume beamformer and the proposed method outperform the INCM-simplified beamformer, the INCM-MEPS beamformer, and the INCM-MCP beamformer. The output of the INCM-SDC beamformer becomes good when the SNR is greater than −20 dB, while the NDL-SMI algorithm decreases with the increase in SNR. Furthermore, the proposed method has the largest output SINR. Figure 6 presents the mean output SINR of the beamformers versus the number of training snapshots for fixed-input SNR. The number of snapshots is varied from 50 to 1000 in increments of 50. The output of the NDL-SMI beamformer changes with the number of snapshots. These results show that, when the number of snapshots is less than 150, the proposed method performs worse than the other algorithms, but when the number of snapshots is more than 150, it performs better. This is because when the ratio of $K$ to the signal frequency is too small, the signal power cannot be correctly estimated using the eigenvalues of $\hat{\mathbf{R}}$. Then, the difference between $\hat{\hat{\mathbf{R}}}_{in}$ and $\mathbf{R}_{in}$ will be significant, which degrades the performance of the proposed method.

**Table 1.** The SNR (dB) estimation results.

| **Input** | −30 | −25 | −20 | −15 | −10 | −5 | 0 | 5 | 10 | 15 | 20 | 25 | 30 |
|---|---|---|---|---|---|---|---|---|---|---|---|---|---|
| **Estimate** | −23.71 | −21.65 | −18.76 | −14.85 | −9.98 | −5.01 | 0.40 | 5.12 | 10.03 | 15.00 | 19.99 | 24.97 | 30.29 |

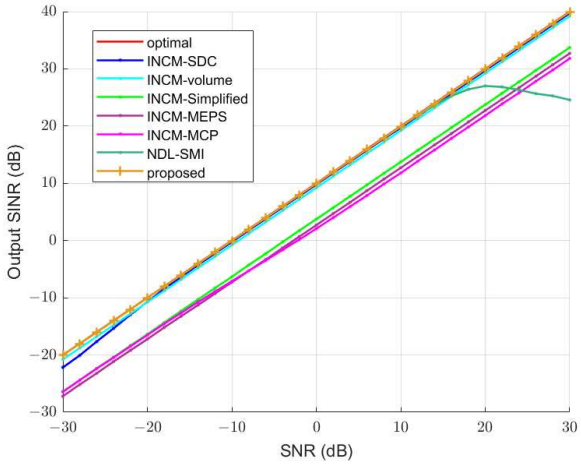


**Figure 4.** Output SINR versus input SNR in the case of known SV.

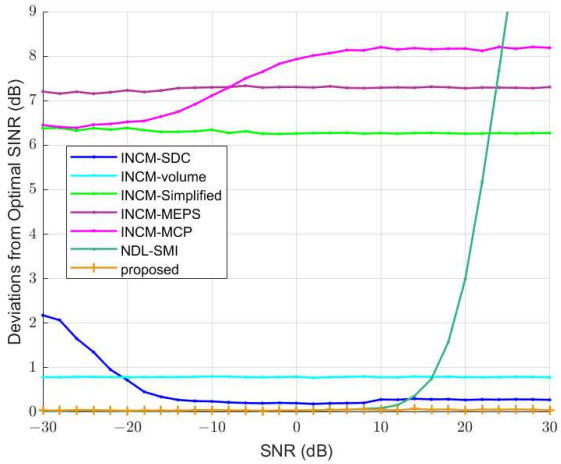


**Figure 5.** Deviation from the optimal SINR in the case of known SV.

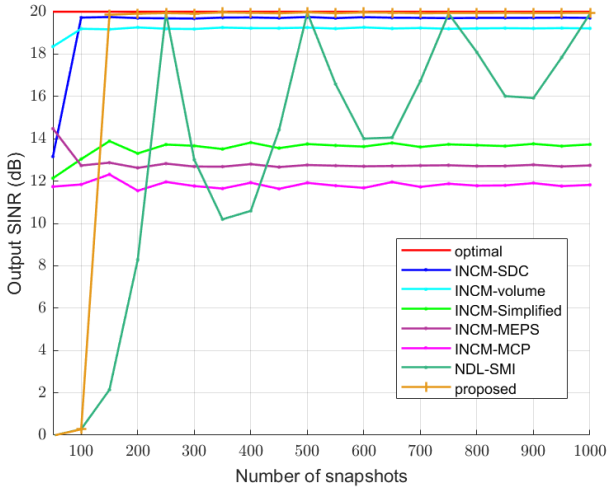


**Figure 6.** Output SINR versus the number of snapshots in the case of known SV.

### *4.2. Case 2: Mismatch Due to Look Direction Error*

In this case, look direction error is considered, and the error $\Delta\theta$ is assumed to be uniformly distributed in $[-4°, 4°]$. All other errors in (38) are set to 0. Figure 7 presents the mean output SINR versus input SNR for the beamformers with a fixed number of snapshots. Further, Figure 8 shows the deviation of each beamformer from the optimal beamformer. This indicates that the proposed method outperforms the others, and the look direction error decreases the output SINR of the INCM-SDC beamformer, the INCM-simplified beamformer, the NDL-SMI beamformer, and the INCM-MCP beamformer. Figure 9 presents the mean output SINR of the beamformers versus the number of snapshots for fixed-input SNR. These results show that, when the number of snapshots is more than 150, the INCM-volume beamformer and the proposed method are more robust to look direction error.

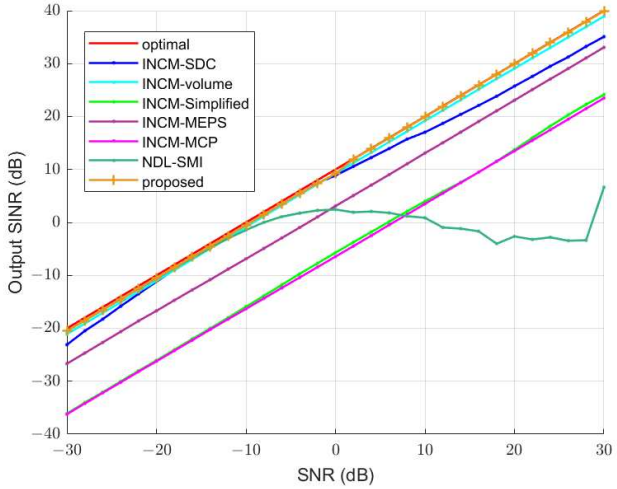


**Figure 7.** Output SINR versus input SNR in the case of look direction error.

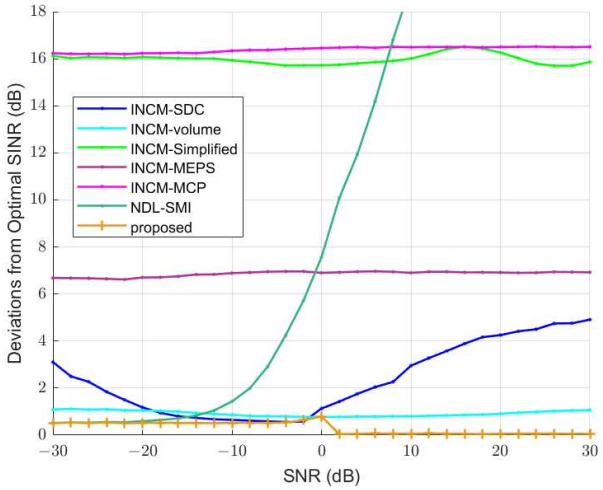


**Figure 8.** Deviation from the optimal SINR in the case of look direction error.

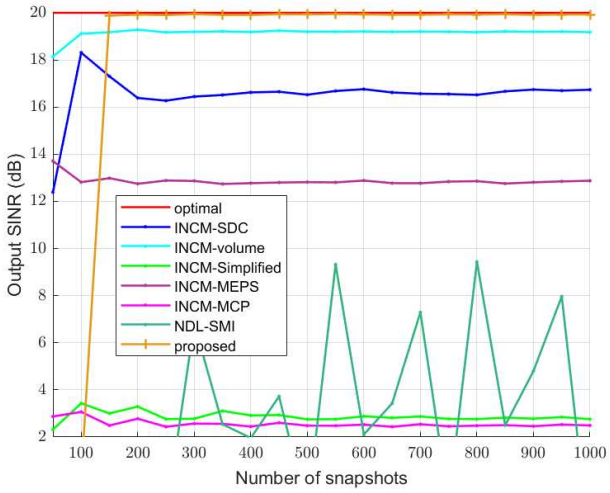


**Figure 9.** Output SINR versus the number of snapshots in the case of look direction error.

### *4.3. Case 3: Mismatch Due to Gain, Phase, and Sensor Location Errors*

In this case, gain error, phase error, and location error are considered. The gain error $\Delta\xi$ and phase error $\Delta\varphi$ are randomly distributed according to $N(0, 0.1^2)$ and $N(0, 0.25\pi^2)$, respectively, and the sensor location error $\Delta d$ is uniformly distributed in the interval $[-0.1, 0.1]$ measured in sensor space. The look direction error is $\Delta\theta = 0$. The mean output SINR versus the input SNR for a fixed number of snapshots is given in Figure 10. Figure 11 shows the deviation of each beamformer from the optimal beamformer. This shows that several methods are insensitive to gain error, phase error, and location perturbation. The result of the proposed method is better than the other techniques. The output SINR versus the number of snapshots for fixed input SNR is given in Figure 12. These results show that the number of snapshots does not have a significant effect on the performance of the beamformers, except the NDL-SMI beamformer, when the number of snapshots is more than 150.

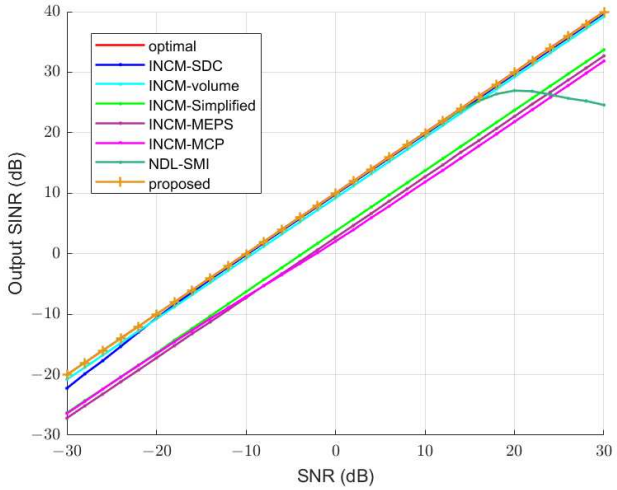


**Figure 10.** Output SINR versus input SNR in the case of gain, phase, and sensor location errors.

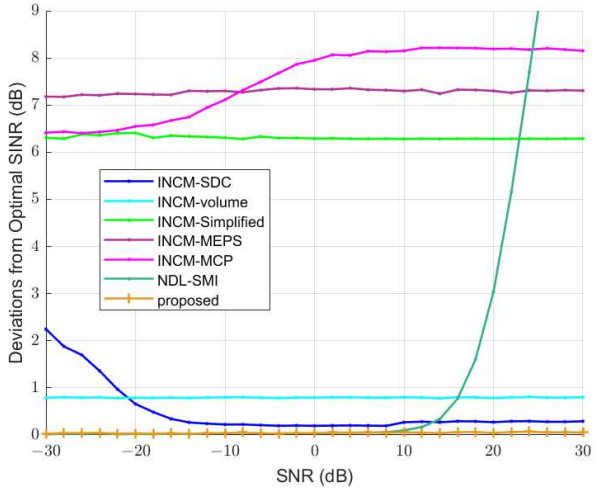


**Figure 11.** Deviation from the optimal SINR in the case of gain, phase, and sensor location errors.

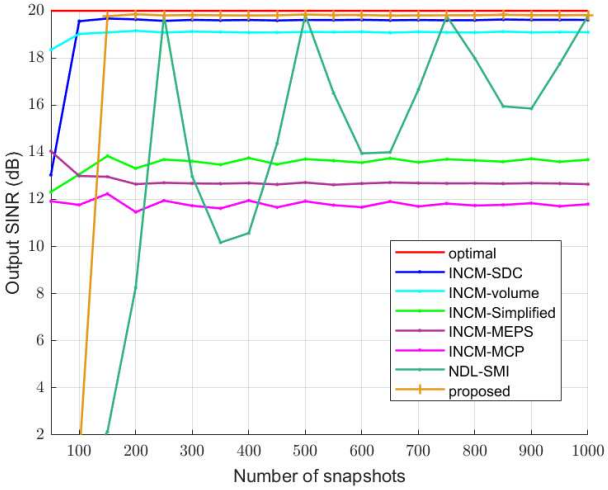


**Figure 12.** Output SINR versus the number of snapshots in the case of gain, phase, and sensor location errors.

### *4.4. Case 4: Mismatch Due to Coherent Local Scattering*

In addition to look direction error, gain error, phase error, and location perturbation, the effect of a mismatch in the desired signal SV caused by coherent local scattering [38] is considered in this case. The desired signal is assumed to follow a direct path and coherently scattered paths, so the SV is modeled as $\mathbf{a} = \mathbf{a}(\theta_1) + \sum_{p=1}^{4} e^{j\varphi_p}\mathbf{a}(\theta_{Lp})$, where $\mathbf{a}(\theta_{Lp})$ is the $p$th coherently scattered path in a direction $\theta_{Lp}$, and all $\theta_{Lp}, p = 1, 2, 3, 4$ are randomly distributed in a Gaussian distribution with mean of $5^\circ$ and standard deviation of $1^\circ$; and $\varphi_p$ represents the path phase, whose value was independently and randomly generated from the $[0, 2\pi]$ interval. The look direction error in this case is uniformly distributed in $[-2^\circ, 2^\circ]$. It should be noted that the look direction mismatch, $\theta_{Lp}$, and $\varphi_p$ changed from run to run but were fixed from snapshot to snapshot.

Figure 13 gives the mean output SINR versus the input SNR for a fixed number of snapshots. Figure 14 presents the deviation of each beamformer from the optimal beamformer. These results show that the proposed method provides the best performance. Figure 15 gives the mean output SINR for the beamformers versus the number of snapshots for a fixed-input SNR. This shows that the output SINR for the proposed method is the highest when the number of snapshots is more than 150.

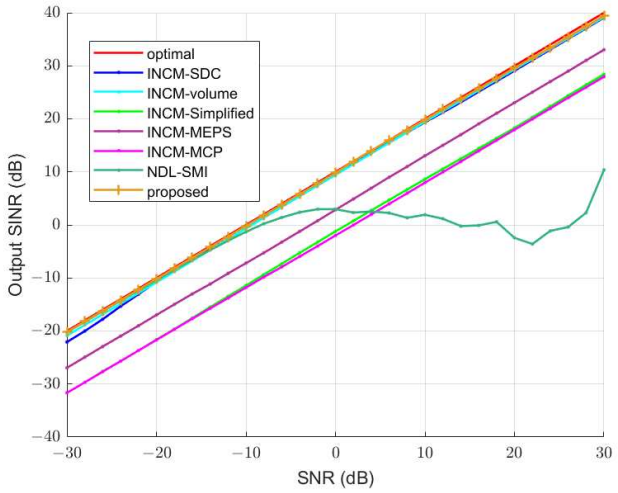


**Figure 13.** Output SINR versus input SNR in the case of coherent local scattering.

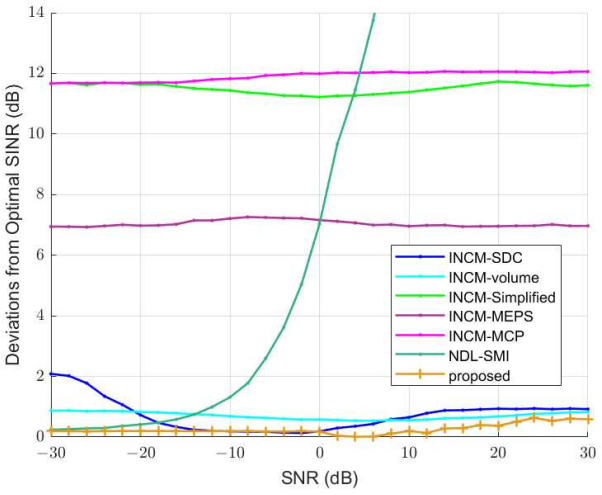


**Figure 14.** Deviations from the optimal SINR in the case of coherent local scattering.

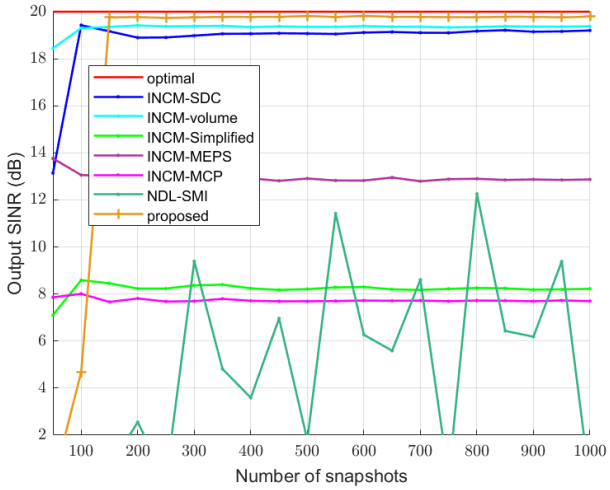


**Figure 15.** Output SINR versus the number of snapshots in the case of coherent local scattering.

### *4.5. Case 5: Validation for Different Numbers of Interferers*

This case validates the beamformers for different numbers of interferers. The number of snapshots is fixed as 2000. The SOI arrives from angle $\theta_1 = 5°$, while the DOA of interferences are random. The information about each interference is shown in Table 2. Figures 16 and 17 give the mean output SINR versus the number of interferers with SNR = $-5$ dB and SNR = 10 dB, respectively. These results show that most algorithms decrease as interference increases, and the proposed method provides better robustness than other beamformers.

**Table 2.** The settings for the interferences.

| **Interference** | 1 | 2 | 3 | 4 | 5 | 6 |
|---|---|---|---|---|---|---|
| **Frequency (kHz)** | 59 | 61 | 59 | 60 | 60.6 | 60.6 |
| **Input INR (dB)** | 30 | 30 | 10 | 10 | 20 | 15 |

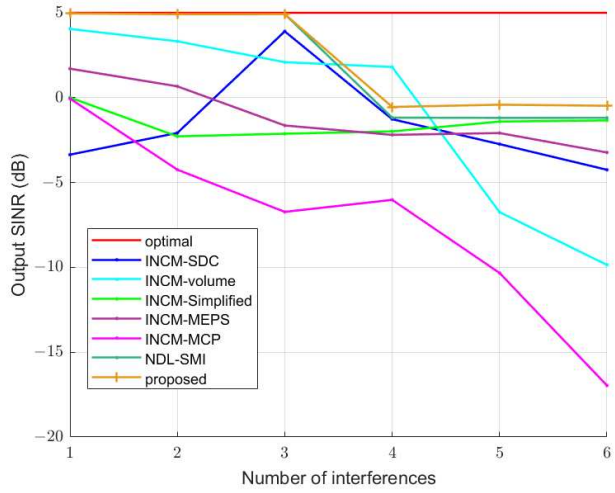


**Figure 16.** Output SINR versus the number of interferers with SNR = $-5$ dB.

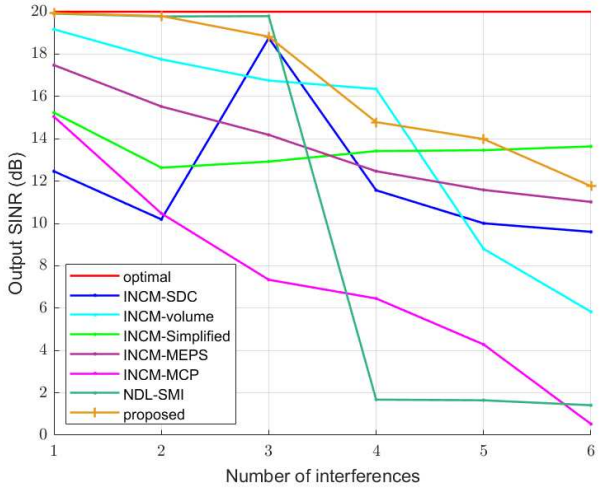


**Figure 17.** Output SINR versus the number of interferers with SNR = 10 dB.

## 5. Conclusions

In this paper, a novel interference-plus-noise covariance matrix (INCM) reconstruction method was proposed for robust adaptive beamforming (RAB). First, an initial SNR estimation algorithm was proposed, and then INCM reconstruction methods were developed according to the SNR. The sample covariance matrix (SCM) is directly used to reconstruct the INCM when the input SNR is low. This preserves the interference and noise information while ignoring the influence of the desired signal. When the input SNR is high, the INCM is reconstructed through interference and noise power estimation via eigenvalues combined with subspace-based interference SV optimization. In addition, the reconstructed INCM is used in the subsequent QCQP problem to estimate the SV of the desired signal. Simulation results were presented which demonstrate that the proposed method achieves a performance superior to other approaches in various model error conditions.

**Author Contributions:** Conceptualization, L.C. and H.Z.; methodology, L.C.; software, L.C.; validation, L.C., H.Z. and T.L.; formal analysis, L.C.; investigation, T.L.; resources, H.Z.; data curation, H.Z.; writing—original draft preparation, L.C.; writing—review and editing, T.A.G.; visualization, L.C.; supervision, H.Z.; project administration, T.L.; funding acquisition, H.Z. All authors have read and agreed to the published version of the manuscript.

**Funding:** This research was funded by the National Natural Science Foundation of China (Grant Nos. 91938204, 41527901, and 61701462), Research Fund for high-level talents of Qingdao Agricultural University.

**Data Availability Statement:** Please contact Hao Zhang at zhanghao@ouc.edu.cn.

**Conflicts of Interest:** The authors declare no conflict of interest.

## References

1. Chen, Z.; Xu, W. Joint passive detection and tracking of underwater acoustic target by beamforming-based Bernoulli filter with multiple arrays. *Sensors* **2018**, *18*, 4022. [CrossRef] [PubMed]
2. Jiang, J.; Wu, Z.; Huang, M.; Xiao, Z. Detection of underwater acoustic target using beamforming and neural network in shallow water. *Appl. Acoust.* **2022**, *189*, 108626. [CrossRef]
3. Foresti, G.L.; Murino, V.; Regazzoni, C.S.; Trucco, A. A voting-based approach for fast object recognition in underwater acoustic images. *IEEE J. Ocean. Eng.* **1997**, *22*, 57–65. [CrossRef]
4. Wang, X.; Liu, A.; Zhang, Y.; Xue, F. Underwater acoustic target recognition: A combination of multi-dimensional fusion features and modified deep neural network. *Remote Sens.* **2019**, *11*, 1888. [CrossRef]
5. Banerjee, S.; Agrawal, M.; Fauziya, F. A Generalized Gaussian noise receiver for improved underwater communication in leptokurtic noise. In Proceedings of the OCEANS 2017, Aberdeen, UK, 19–22 June 2017.
6. Luo, H.; Wu, K.; Ruby, R.; Liang, Y.; Guo, Z.; Ni, L.M. Software-defined architectures and technologies for underwater wireless sensor networks: A survey. *IEEE Commun. Surv. Tutor.* **2018**, *20*, 2855–2888. [CrossRef]

7. Luo, H.; Wu, K.; Ruby, R.; Hong, F.; Guo, Z.; Ni, L.M. Simulation and experimentation platforms for underwater acoustic sensor networks: Advancements and challenges. *ACM Comput. Surv.* **2017**, *50*, 1–44. [CrossRef]
8. Koutrouvelis, A.I.; Hendriks, R.C.; Heusdens, R.; Jensen, J. A convex approximation of the relaxed binaural beamforming optimization problem. *IEEE/ACM Trans. Audio Speech Lang. Process.* **2018**, *27*, 321–331. [CrossRef]
9. Li, J.; Bai, Y.; Zhang, Y.; Qu, F.; Wei, Y.; Wang, J. Cross power spectral density based beamforming for underwater acoustic communications. *Ocean. Eng.* **2020**, *216*, 107786. [CrossRef]
10. Li, J.; Wang, J.; Wang, X.; Qiao, G.; Luo, H.; Gulliver, T.A. Optimal beamforming design for underwater acoustic communication with multiple unsteady sub-Gaussian interferers. *IEEE Trans. Veh. Technol.* **2019**, *68*, 12381–12386. [CrossRef]
11. Van Trees, H.L. *Detection, Estimation, and Modulation Theory Part IV, Optimum Array Processing*; Wiley: New York, NY, USA, 2004.
12. Luan, M.; Wang, B.; Chang, Z.; Hämäläinen, T.; Hu, F. Robust Beamforming Design for RIS-Aided Integrated Sensing and Communication System. *IEEE Trans. Intell. Transp. Syst.* **2023**, *24*, 6227–6243. [CrossRef]
13. Capon, J. High-resolution frequency-wavenumber spectrum analysis. *Proc. IEEE* **1969**, *57*, 1408–1418. [CrossRef]
14. Vorobyov, S.A.; Gershman, A.B.; Luo, Z.Q. Robust adaptive beamforming using worst-case performance optimization: A solution to the signal mismatch problem. *IEEE Trans. Signal Process.* **2003**, *51*, 313–324. [CrossRef]
15. Zhang, M.; Chen, X.; Zhang, A. A simple tridiagonal loading method for robust adaptive beamforming. *Signal Process.* **2019**, *157*, 103–107. [CrossRef]
16. Li, H.; Geng, J.; Xie, J. Robust adaptive beamforming based on covariance matrix reconstruction with RCB principle. *Digit. Signal Process.* **2022**, *127*, 103565. [CrossRef]
17. Carlson, B.D. Covariance matrix estimation errors and diagonal loading in adaptive arrays. *IEEE Trans. Aerosp. Electron. Syst.* **1988**, *24*, 397–401. [CrossRef]
18. Elnashar, A.; Elnoubi, S.M.; El-Mikati, H.A. Further Study on Robust Adaptive Beamforming With Optimum Diagonal Loading. *IEEE Trans. Antennas Propag.* **2006**, *54*, 3647–3658. [CrossRef]
19. Zhuang, J.; Ye, Q.; Tan, Q.; Ali, A.H. Low-complexity variable loading for robust adaptive beamforming. *Electron. Lett.* **2016**, *52*, 338–340. [CrossRef]
20. Jia, W.; Jin, W.; Zhou, S.; Yao, M. Robust adaptive beamforming based on a new steering vector estimation algorithm. *Signal Process.* **2013**, *93*, 2539–2542. [CrossRef]
21. Huang, F.; Sheng, W.; Ma, X. Modified projection approach for robust adaptive array beamforming. *Signal Process.* **2012**, *92*, 1758–1763. [CrossRef]
22. Feldman, D.D.; Griffiths, L.J. A projection approach for robust adaptive beamforming. *IEEE Trans. Signal Process.* **1994**, *42*, 867–876. [CrossRef]
23. Wang, J.; Zhang, W.; Liu, W. Minimum sensitivity based robust beamforming with eigenspace decomposition. *Multidimens. Syst. Signal Process.* **2018**, *29*, 687–701. [CrossRef]
24. Feng, Y.; Liao, G.; Xu, J. Robust adaptive beamforming against large steering vector mismatch based on minimum dispersion. *Digit. Signal Process.* **2020**, *99*, 102676. [CrossRef]
25. Gu, Y.; Leshem, A. Robust adaptive beamforming based on interference covariance matrix reconstruction and steering vector estimation. *IEEE Trans. Signal Process.* **2012**, *60*, 3881–3885.
26. Zhang, Z.; Liu, W.; Leng, W.; Wang, A.; Shi, H. Interference-plus-noise covariance matrix reconstruction via spatial power spectrum sampling for robust adaptive beamforming. *IEEE Signal Process. Lett.* **2015**, *23*, 121–125. [CrossRef]
27. Zheng, Z.; Yang, T.; Wang, W.Q.; So, H.C. Robust Adaptive Beamforming via Simplified Interference Power Estimation. *IEEE Trans. Aerosp. Electron. Syst.* **2019**, *55*, 3139–3152. [CrossRef]
28. Mohammadzadeh, S.; Nascimento, V.H.; De Lamare, R.C.; Kukrer, O. Robust adaptive beamforming based on power method processing and spatial spectrum matching. In Proceedings of the ICASSP 2022—2022 IEEE International Conference on Acoustics, Speech and Signal Processing (ICASSP), Singapore, 23–27 May 2022; pp. 4903–4907.
29. Reed, I.S.; Mallett, J.D.; Brennan, L.E. Rapid Convergence Rate in Adaptive Arrays. *IEEE Trans. Aerosp. Electron. Syst.* **1974**, *10*, 853–863. [CrossRef]
30. Chang, L.; Yang, H.; Gulliver, T.A.; Tan, S.; Wang, Y. Large Direction-of-Arrival Mismatch Correction for Adaptive Beamforming. *IEEE Access* **2022**, *10*, 61201–61212. [CrossRef]
31. Zhu, X.; Xu, X.; Ye, Z. Robust adaptive beamforming via subspace for interference covariance matrix reconstruction. *Signal Process.* **2020**, *167*, 107289. [CrossRef]
32. Huang, L.; Zhang, J.; Xu, X.; Ye, Z. Robust adaptive beamforming with a novel interference-plus-noise covariance matrix reconstruction method. *IEEE Trans. Signal Process.* **2015**, *63*, 1643–1650. [CrossRef]
33. Mohammadzadeh, S.; Nascimento, V.H.; de Lamare, R.C.; Kukrer, O. Maximum entropy-based interference-plus-noise covariance matrix reconstruction for robust adaptive beamforming. *IEEE Signal Process. Lett.* **2020**, *27*, 845–849. [CrossRef]
34. Suleesathira, R. Robust null broadening beamforming based on adaptive diagonal loading for look direction mismatch. In Proceedings of the 2021 13th International Conference on Knowledge and Smart Technology (KST), Bangsaen, Thailand, 21–24 January 2021; pp. 49–54.
35. Sun, S.; Ye, Z. Robust adaptive beamforming based on a method for steering vector estimation and interference covariance matrix reconstruction. *Signal Process.* **2021**, *182*, 107939. [CrossRef]

36. Yang, J.; Tu, Y.; Lu, J.; Yang, Z. Robust adaptive beamforming based on subspace decomposition, steering vector estimation and correction. *IEEE Sens. J.* **2022**, *22*, 12260–12268. [CrossRef]
37. Grant, M.; Boyd, S. *CVX: Matlab Software for Disciplined Convex Programming*, version 2.1; Springer: Berlin/Heidelberg, Germany, 2014.
38. Goldberg, J.; Messer, H. Inherent limitations in the localization of a coherently scattered source. *IEEE Trans. Signal Process.* **1998**, *46*, 3441–3444. [CrossRef]